THE SUPER-HOT THERMAL COMPONENT IN THE DECAY PHASE OF SOLAR FLARES

HUA-AN LIN

Space Physics Institute, Chinese Academy of Sciences, Beijing, China and Space Sciences Laboratory, University of California, Berkeley, CA 94720, U.S.A.

and

R. P. LIN and S. R. KANE

Space Sciences Laboratory, University of California, Berkeley, CA 94720, U.S.A.

(Received 12 April; in revised form 9 August, 1985)

Abstract. Solar X-ray observations from balloons and from the SMM and HINOTORI spacecraft have revealed evidence for a super-hot thermal component with a temperature of $\gtrsim 3 \times 10^7$ K in many solar flares, in addition to the usual $10–20 \times 10^6$ K soft X-ray flare plasma. We have systematically studied the decay phase of 35 solar flare X-ray events observed by ISEE-3 during 1980. Based on fits to the continuum X-ray spectrum in the 4.8–14 keV range and to the intensity of the 1.9 Å feature of iron lines, we find that 15 (about 43%) of the analyzed events have a super-hot thermal component in the decay phase of the flare. In this paper the important properties of the super-hot thermal component in the decay phase are summarized. It is found that an additional input of energy is required to maintain the super-hot thermal components. Finally, it is suggested that the super-hot thermal component in the decay phase is created through the reconnection of the magnetic field during the decay phase of solar flares.

1. Introduction

As is well known, there exist two components of solar X-rays in flares, soft X-rays with energy < 15 keV and hard X-rays with energy > 15 keV. These two components have completely different spatial, temporal, and spectral structure. Soft X-rays with an exponential spectrum are usually interpreted as thermal bremsstrahlung from an isothermal plasma ($T \sim 1 - 2 \times 10^7$ K) at the top of flare loops. Hard X-rays with a single or double power-law spectrum can be explained as non-thermal bremsstrahlung from energetic non-thermal electrons stopping in relatively cold plasma at the footpoints of flare loops (Arnoldy *et al.*, 1968; Brown, 1972; Lin and Hudson, 1971, 1976). Another interpretation assumes that hard X-rays are thermal emission with an exponential spectrum from a plasma with electron temperature $T \geq 10^8$ K (Chubb *et al.*, 1966; Brown, 1975).

Recently, a new component whose X-ray spectrum includes both soft (< 15 keV) X-rays and hard (> 15 keV) X-rays has been identified in solar flares. From an intense flare on June 27, 1980, Lin *et al.* (1981) found a near isothermal component with temperature $T \sim 34 \times 10^6$ K through the measurements with a balloon-borne array of germanium detectors with very high spectral resolution (≤ 1 keV). At the same time, the usual $10–20 \times 10^6$ K soft X-ray thermal emission was also present. We call this new component the 'super-hot thermal component' (shortened to 'SHTC') to distinguish it from the usual soft X-ray thermal emission.

Solar Physics **99** (1985) 263–275. 0038–0938/85.15.

Several flares observed by the Hard X-Ray Imaging Spectrometer (HXIS – Van Beek *et al.*, 1980) on SMM indicated the presence of a hot plasma component with a temperature of about 40×10^6 K or higher. For example, Hoyng *et al.* (1981) described and analyzed a two-ribbon flare on May 21, 1980. It turned out that, in the thermal phase, the two-temperature model fits the HXIS spectrum rather well, and a hot component temperature of 7×10^7 K and a cool-component temperature of 2×10^7 K were found just after the impulsive phase. For the solar flare on April 10, 1980, Machado *et al.* (1982) found, by fitting the low energy channels with the one-temperature model, that significant discrepancies appear in the high energy channels where the observed number of counts was much larger than predicted. The excess number of counts could be explained by thermal contribution from a high-temperature, low emission measure plasma. A high-temperature component with $T = 6 \times 10^7$ K and emission measure $EM = 4 \times 10^{46}$ cm^{-3} was found about one minute after the peak of hard X-rays. For some gradual bursts of long duration observed with the hard X-ray imaging (SXT) and spectrometer (HXM) instruments on the HINOTORI satellite, it has been shown that, although the photon spectrum in the late phase of most gradual bursts was basically a power-law from the very beginning through the end of the events, the 30–40 keV channel had some excess flux above the power-law extrapolation from the higher energies. This excess was explained by the existence of a different thermal component (Ohki *et al.*, 1983).

In all of the flares mentioned above, an SHTC appeared in the decay phase of the events. Compared with the usual hot thermal component, what are the properties of SHTC? What is the possible mechanism for the production of SHTC? In this paper we try to answer these questions through a systematic analysis of thirty-five events observed by the X-ray spectrometer on the ISEE-3 (Third International Sun–Earth Explorer) during 1980.

2. Instrumentation

The X-ray spectrometer experiment aboard ISEE-3 consists of two X-ray detectors, a proportional counter (5–14 keV) and a NaI (TL) scintillator (12–1250 keV).

Assume that the solar flare X-rays are emitted by two isothermal plasmas. If E_{TB} is the breakpoint energy where the X-ray photon flux from high temperature T_H plasma is equal to the flux from low temperature T_L plasma, then

$$\frac{E_{TB}}{KT_H} = \frac{\ln\left[\frac{EM_L}{EM_H}\left(\frac{T_H}{T_L}\right)^{1/2}\right]}{\left(\frac{T_H}{T_L} - 1\right)}, \tag{1}$$

where T_H, EM_H, T_L, and EM_L are temperature and emission measure of high and low temperature plasmas, respectively, and K is Boltzman's constant. Figure 1 shows the

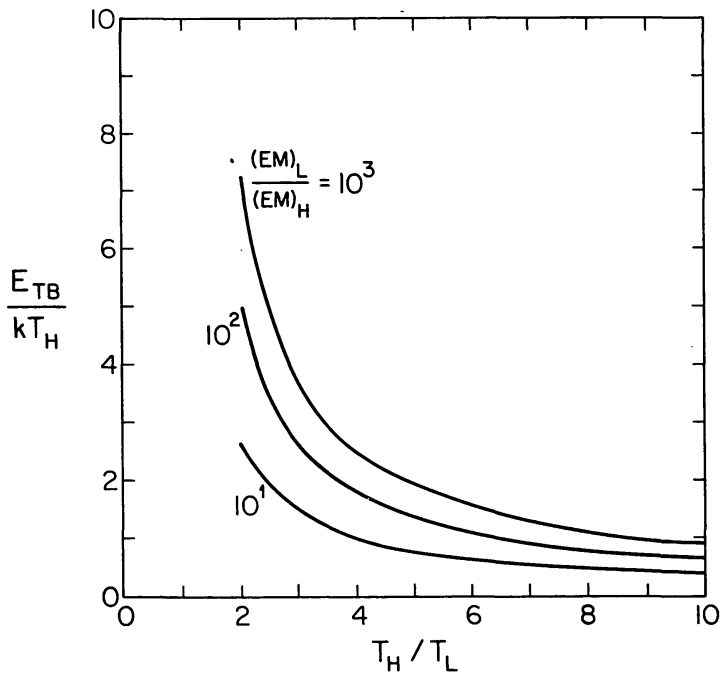

Fig. 1. The relationship between the break point energy E_{TB} and the parameters of the two-temperature model. Usually, the ratio of temperatures $T_H/T_L = 2$–5 and the ratio of emission measures $EM_L/EM_H = 10^2$–10^3. The break point energy E_{TB} is usually around 10 keV.

relationship between E_{TB}/KT_H and T_H/T_L with EM_L/EM_H as a parameter. Typically it appears $T_H/T_L = 2$–5 and $EM_L/EM_H = 10^2$–10^3. Since $T_L \sim 10$–20×10^6 K in Figure 1, we find that the breakpoint energy E_{TB} is usually near 10 keV. For ISEE-3 X-ray experiments the breakpoint energy falls within the range of the proportional counter. The proportional counter is 1.27 cm in diameter and filled with a mixture of 97% xenon and 3% CO_2 to a pressure of one atmosphere. The central part of the counter body is made of 0.51 mm thick, 1.27 cm wide beryllium covered with 25.4 μm thick aluminum and serves as the X-ray entrance window. The field of view of the proportional counter determined by a magnesium collimator is $\approx 360°$ in the ecliptic plane and $\approx 10°$ FWHM in a direction perpendicular to the ecliptic.

The energy range observed by the proportional counter is divided into six energy intervals (referred to as PC1 TO PC6): 4.8 to 5.8; 5.8 to 6.9; 6.9 to 8.2; 8.2 to 9.7; 9.7 to 11.8; and 11.8 to 14.0 keV. These energy intervals are determined by on-board calibration and are somewhat different from the nominal values set before the launch of ISEE-3. A more complete description of the instruments has been given by Anderson *et al.* (1978) and Kane *et al.* (1982).

For a theoretical X-ray spectrum $F(E)$ (photon cm^{-2} s^{-1} keV^{-1}) the counting rate of the Jth channel is given by $N_{CL}(J)$:

$$N_{CL}(J) = \int_{\Delta E_j} S(J, E)\, F(E)\, \mathrm{d}E \quad (\mathrm{cs}^{-1}) \tag{2}$$

where ΔE_J is the energy width of the Jth channel and $S(J, E)$ is the response function

of the proportional counter expressed as effective area in cm^2, as shown in Figure 2.

In order to avoid distortion of the observed X-ray spectrum due to the space charge effect in the proportional counter during large events, only those events for which the total counting rate is $< 10^4\ cs^{-1}$ are analyzed. These events were mostly subflares. Some of them are shown in Figure 3.

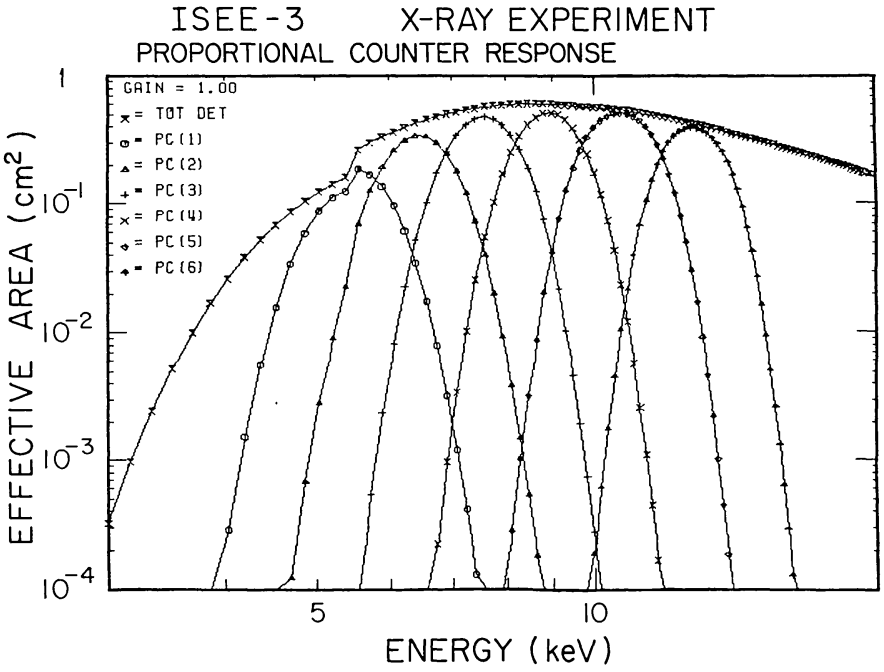

Fig. 2. The effective area (cm^2) for each channel of the ISEE-3 X-ray proportional counter.

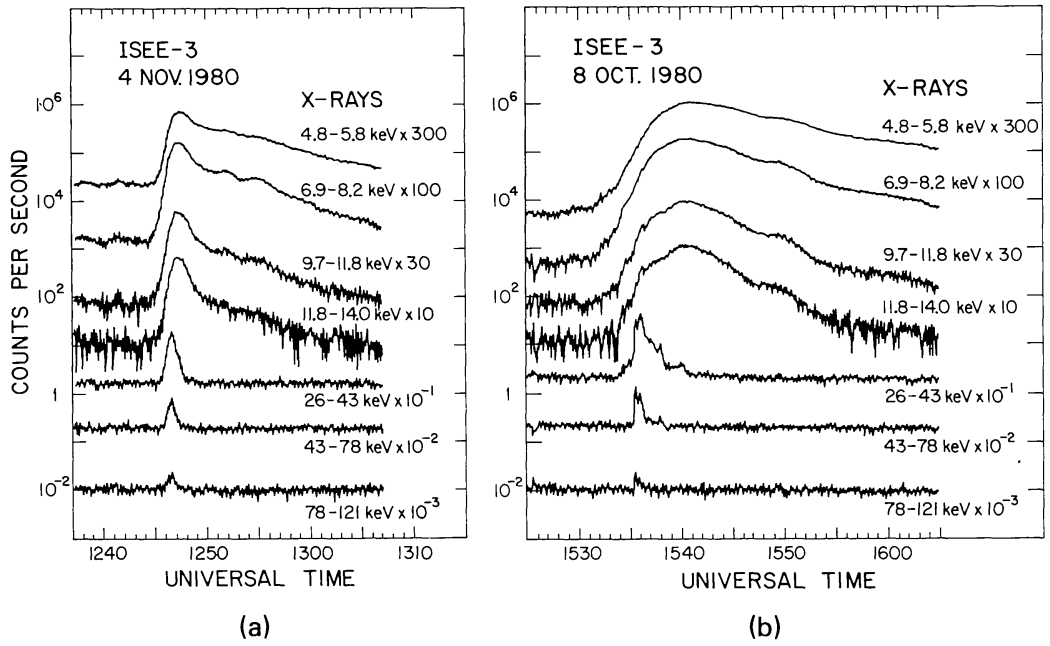

Fig. 3. The counting rate versus time profiles for two solar flare X-ray bursts: (a) 4 November, 1980; (b) 8 October, 1980.

3. Data Analysis

Each selected solar X-ray event is fit to two models. Model one is a one-temperature model which has two fitting parameters: electron temperature T and emission measure EM. For the one-temperature model, the differential X-ray spectrum with $g(E, T) = 1$ and $f(E, T) = 0$ (Culhane and Acton, 1970) is given by

$$F(E) = 6.84 \times 10^{-39} E^{-1} T^{-1/2}(EM) \exp\left(-\frac{E}{KT}\right) (\text{photon cm}^{-2}\,\text{s}^{-1}\,\text{keV}^{-1}), \tag{3}$$

where T is in degrees kelvin, E is the photon energy in keV, and EM is in cm^{-3}. In the numerical constant 6.84×10^{-39}, a factor of $\overline{Z}^2 = 1.8$ is incorporated to account for solar coronal abundances. Model two is a two-temperature model which has four fitting parameters to account for the low and high temperature components: T_L, EM_L, T_H, and EM_H. The expression for the X-ray spectrum of model two is a sum of single-temperature differential spectra (3).

In the data analysis, the minimum averaging time of the counting rate has been chosen to be 16 s in order to obtain good statistical accuracy in the high energy channel. The quiescent background emission from the pre-flare data averaged over 2 min have been subtracted from the data used for fitting. From Figure 2 it can be seen that the 1.9 Å feature ($E_I = 6.50$ keV) contributes mainly to PC2, although some of the counts appear also in PC3. In the fitting procedure we have deleted channel 2 and retained channel 3. Then optimum values of the parameters were obtained by requiring the minimum reduced chi-square χ_v^2,

$$\chi_v^2 = \frac{1}{n-m} \sum_{i=1}^{n} \frac{(I_i - F_i)^2}{\sigma_i^2}, \tag{4}$$

where n, the number of data points used in fitting, is 5 and m is the number of fitting parameters ($m = 2$ for one-temperature fit and $m = 4$ for two-temperature fit). F_i and σ_i are, respectively, the computed value and the standard deviation corresponding to an observed value I_i due to the random fluctuations in the count rates only.

The values of reduced χ_v^2 for the two-model fits are 10 to 100 in the decay phase of flares. Taking into account the contribution of the iron line (1.9 Å) to channel 3, which is estimated to be about $(30 \pm 10)\%$ of the total counting rates in channel 3, and the uncertainties in the instrument response function $S(J, E)$, which are estimated to be about $\pm 5\%$, the reduced χ_v^2 would be decreased by a factor of 5 to 30.

The emission feature at 1.9 Å consists of the resonance, intersystem, and forbidden lines of the helium-like Fe XXV ion plus the contribution from collisional excitation and dielectronic recombination in Fe XXIV and below. In the lower temperature range of $5–20 \times 10^6$ K the 1.9 Å feature is dominated by emissions in lower stages of ionization (Fe XXIII – Fe XVIII). As the temperature increases, the fractional abundance of the ions in lower ionization stages decreases rapidly (Jacobs *et al.*, 1977), so the contribution

from lower ionization stages can be ignored in the high temperature range. The theoretical intensity of the 1.9 Å feature which is used in this paper consists of three parts, as shown in Figure 4. For temperatures between 8–18 × 10^6 K, we adopt the results calculated by Parkinson *et al.* (1979) and use them with the atomic parameters of Merts *et al.* (1976). This part takes account of the contribution from Fe XXV – Fe XVIII. For temperatures higher than 30 × 10^6 K, the results are calculated with the data and formulae provided by Acton *et al.* (1977) and used with the results of Bhalla *et al.* (1975). This part considers only the contribution from Fe XXV – Fe XXIV. The results for temperatures in the range 18–30 × 10^6 K were obtained by a smooth interpolation.

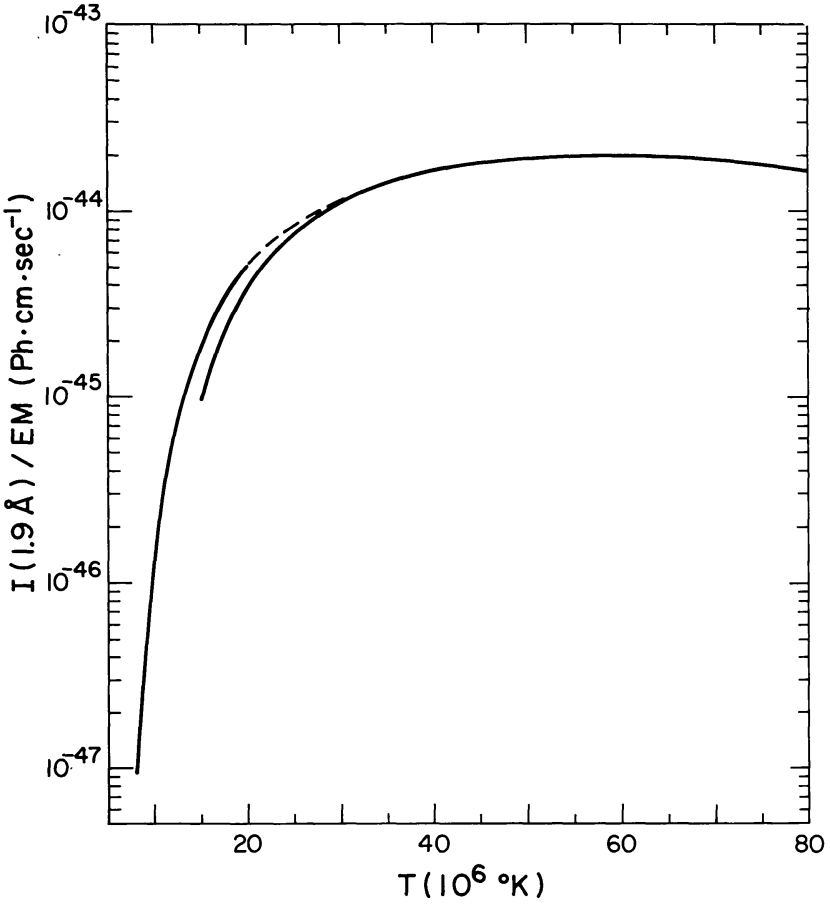

Fig. 4. The theoretical intensity of the 1.9 Å feature of iron lines per unit emission measure for a thermal plasma. For T = 8–18 × 10^6 K, the results of Merts *et al.* (1976) are used. For $T > 30 \times 10^6$ K, the results of Bhalla *et al.* (1975) are used. For T = 18–30 × 10^6 K, the results are obtained by smooth interpolation.

We compare the one-temperature and two-temperature model fits using two factors, χ^2_R and I_R (.9), where χ^2_R is the ratio of the reduced chi-square χ^2_v for the single temperature model to that for the two-temperature model, and I_R (1.9) is the ratio of the theoretically computed intensity to the observed intensity of the 1.9 Å feature. These two factors are used to judge which model fits better to the observations.

The observed intensity of the 1.9 Å feature is given by

$$I_{OS}(1.9) = \left.\frac{N_{OS}(J) - N_{CL}(J)}{S(J, E_I)}\right|_{J=2} \text{(photon cm}^{-2}\text{ s}^{-1}\text{)}, \tag{5}$$

where $N_{OS}(J)$ is the observed counting rate in the Jth channel and $N_{CL}(J)$ is the calculated continuum counting rate from Equation (2). $S(J, E_I)$ is the effective area (Figure 2) of the Jth channel at $E_I = 6.50$ keV. The expected theoretical intensity of the 1.9 Å feature can be deduced from Figure 4. For the two-temperature model fit, the theoretical intensity of the 1.9 Å feature is the sum of the two components corresponding to the high and low temperature emissions.

Two examples of the results obtained with this fitting procedure are shown in Figure 5. $\chi_R^2 < 1$ implies the one-temperature fit is better than the two-temperature fit,

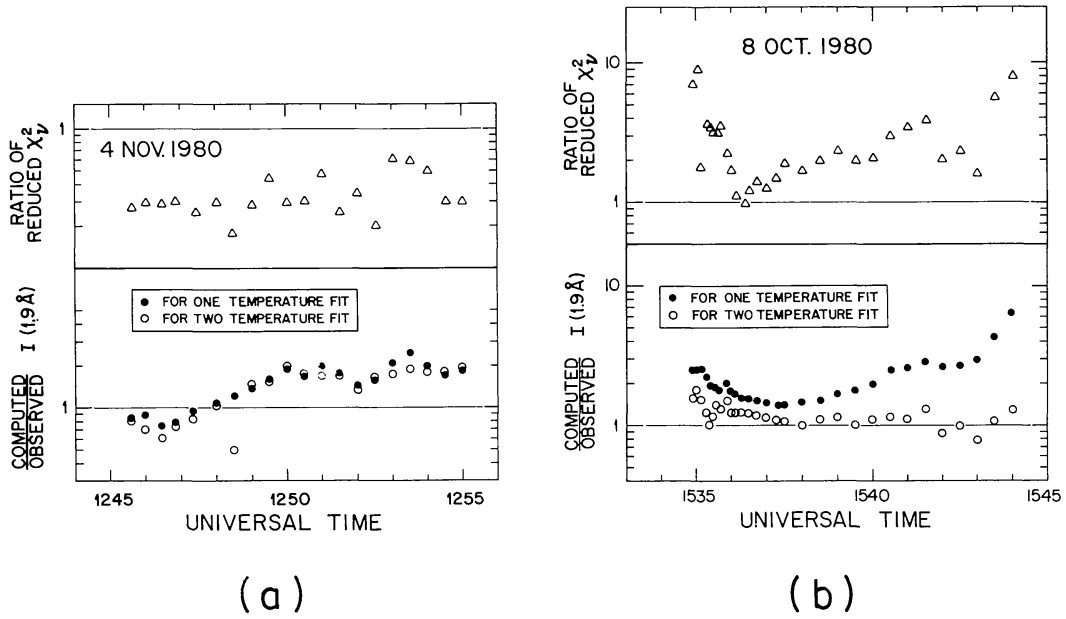

Fig. 5. Results of fitting procedure for two selected events: (a) 4 November 1980; (b) 8 October, 1980. $\chi_R^2 < 1$ implies that a one-temperature fit is better than a two-temperature fit, and vice versa. Note that, in the $\chi_R^2 > 1$ case, the I_R (1.9) for the two-temperature fit are always closer to 1. On the other hand, in the $\chi_R^2 < 1$ case the I_R (1.9) for both models fits are almost the same.

and vice versa if $\chi_R^2 > 1$. The non-thermal component from hard X-rays (power-law spectrum) in the impulsive phase may cause additional counts in the higher energy channel of the proportional counter that would distort the results of thermal spectrum analysis. In this paper we limit our analysis to the decay phase when the effect of the non-thermal component can be ignored.

In the $\chi_R^2 < 1$ case (Figure 5a) it can be seen that the I_R (1.9) for the one-temperature fit are almost equal to the ones for the two-temperature fit. In the $X_R^2 > 1$ case (Figure 5b) the I_R (1.9) for the two-temperature fit are closer to 1 than for the one-

temperature fit. Thus in the $\chi_R^2 > 1$ case, the two-temperature model not only fits better with the thermal continuum spectrum, but also improves the estimation of the iron lines (1.9 Å feature). It appears that the two factors, χ_R^2 and I_R (1.9), are sufficient criteria to judge which model is more suitable to describe the emission process happening in the observed events. For instance, the event on 4 November, 1980 (Figures 3a and 5a) is identified as a flare without SHTC occurring in the flare process. On the other hand, in the event on 8 October, 1980 (Figures 3b and 5b), there appears to be an SHTC in the flare.

4. Results

The thirty-five ISEE-3 X-ray spectrometer events during 1980 have been analyzed by the procedures described in the last section. It has been found that fifteen events (about 43% of all the analyzed events) had an SHTC in the decay phase of the flare. Two examples of decay phase super-hot events are shown in Figures 6 and 7. The solar flare on 1980, July 26 (Figure 6a) started at 01 : 17 UT and reached maximum at 01 : 19 UT. Its optical importance was $-N$ and it was located at S07 E53 in Hale plage region 17008. A simple microwave burst with gradual rise and fall started at 01 : 18 UT and reached maximum at 01 : 20 UT (*Solar Geophysical Data*, 1982, No. 460). The hard X-ray burst started at $\sim$01 : 16 : 30 UT and lasted till $\sim$01 : 23 UT (visible in the 26–43 keV channel). Figure 6c is the analysis results of temperature structure for the one-temperature fit (T_U), and two-temperature fit (T_H and T_L), respectively. The noteworthy point is that the high temperature component (T_H) had completely different variation patterns before and after about 01 : 26 UT, just at the time that χ_R^2 changes from less than 1 to larger than 1 (Figure 6b). Before 01 : 26 UT there is no need for an SHTC, as indicated by the close correspondence of T_U and T_L, so T_H shows wild excursions. By comparing Figure 6b with Figure 6c, it appears that for this flare the SHTC began at $\sim$01 : 26 UT, about 7 min later than the flare maximum. The temperature, emission measure and energy content ($EC = 4.13 \times 10^{-16}$ (EM)T) are shown in Figures 6d and 6e. From these plots it can be seen that the emission measure of the usual hot thermal component increased systematically until the appearance of the SHTC.

The solar flare on 15 January, 1980 (Figure 7a) started at 12 : 58 UT and reached maximum at 12 : 59 UT, reported by observation of solar radio emission (*Solar Geophysical Data*, 1980, No. 431), but no associated Hα flare was reported. According to solar X-ray observation by ISEE-3, this flare probably started at $\sim$12 : 58 UT, consistent with the observation of solar radio emission. The hard X-ray burst consisted of two distinguishable peaks at $\sim$12 : 59 : 30 UT and $\sim$12 : 59 : 54 UT, respectively, followed by a slow decay lasting till $\sim$13 : 02 : 30 UT (visible in 26–43 keV). The soft X-ray burst reached a maximum at 13 : 01 UT, about one minute later than the second peak of hard X-rays. From 13 : 00 UT to 13 : 03 UT, the total counting rates of the proportional counter exceeded 10^4 cs^{-1} and tended towards saturation. In this period the results of spectral analysis are not reliable. From Figure 7b it seems that for this flare the SHTC appeared just after the impulsive phase. The temperature and emission measure of this event are shown in Figure 7c.

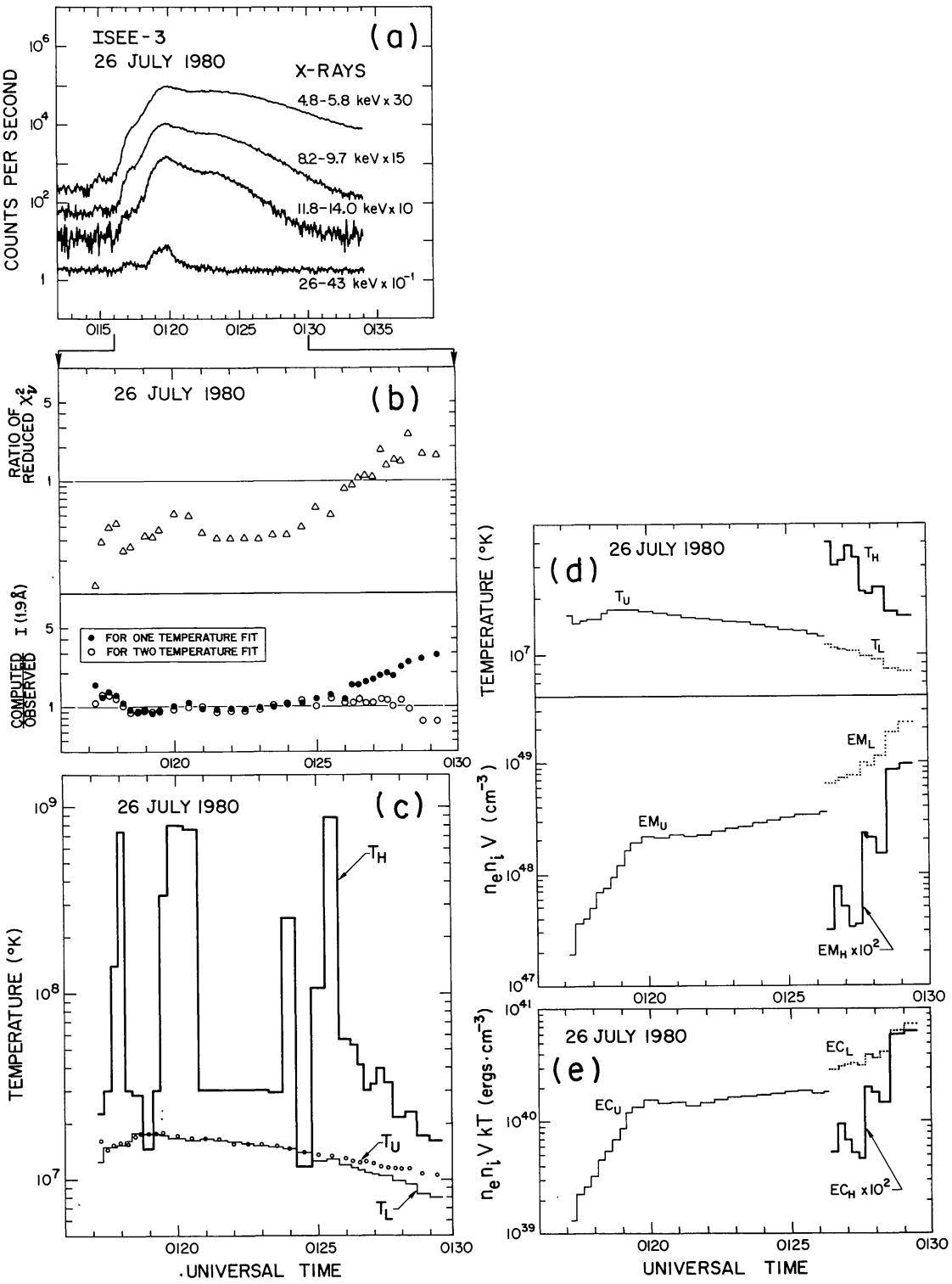

Fig. 6. The decay phase super-hot event on 26 July, 1980. (a) The counting rate versus time profiles for the X-ray burst. (b) The χ^2_R and I_R (1.9) values of the fitting procedure. Note that at about 01 : 26 UT the χ^2_R changes from less than 1 into larger than 1 and after that time the I_R (1.9) for the two-temperature fit becomes closer to 1 than for the one-temperature fit. (c) The analysis results of temperature structure for the one-temperature fit (T_U), and for the two-temperature fit (T_H and T_L), respectively. Note that the high-temperature component (T_H) has a completely different variation pattern before and after 01 : 26 UT. (d) The evolution in time of the electron temperature (T_U, T_H, and T_L) and the emission measure (EM_U, EM_H, and EM_L). (e) The evolution in time of the energy content (EC_U, EC_H, and EC_L). Subscripts: L for the low-temperature component, H for the super-hot thermal component, and U for the usual-temperature component.

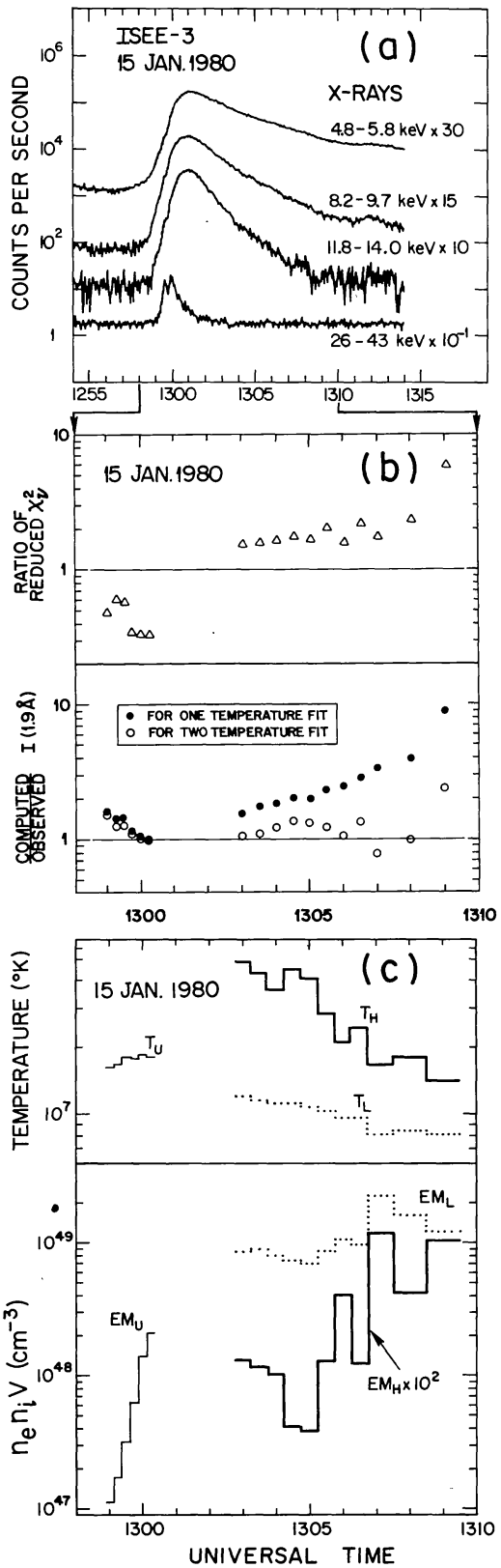

Fig. 7. The decay phase super-hot event on 15 January, 1980. (a) The counting rate versus time profiles for the X-ray burst. (b) The χ_R^2 and I_R (1.9) values of fitting procedure. From 13 : 00 UT to 13 : 03 UT the total counting rates are in excess of $10^4\,\mathrm{cs}^{-1}$. For this event it seems the SHTC appears just after the impulsive phase. (c) The evolution in time of electron temperature (T_U, T_H, and T_L) and the emission measure (EM_U, EM_H, and EM_L). Subscripts: L for the low-temperature component, H for the super-hot thermal component, and U for the usual-temperature component.

The important properties of the decay phase SHTC obtained from Figures 6 and 7, and from other analyzed events, can be summarized as follows:

(1) A decay phase SHTC may occur in both impulsive (Figure 7), and gradual (non-impulsive, Figure 6) events.

(2) The decay phase SHTC may appear at any time in the decay phase from just after the impulsive phase to several minutes later, and last for a long time (~ 10 min). It seems that the more intense an impulsive event is, the earlier the SHTC occurs.

(3) From the energy content (Figure 6e), it appears that the emergence of SHTC is accompanied by the input of additional energy.

(4) Compared with the low-temperature component the SHTC fluctuates more severely in both the electron temperature and emission measure, though in each case the general tendency of electron temperature is to decrease exponentially with time.

(5) For both the low-temperature component and SHTC in the decay phase super-hot event, the general tendency is that the electron temperature drops gradually while the emission measure is rising. It is quite different from the single-temperature structure event, in which both the electron temperature and emission measure are usually decreasing in the later decay phase.

(6) The temperature decay time is about 150–350 s for the decay phase SHTC and about 500–700 s for the low-temperature component. The maximum electron temperature of the decay phase SHTC is about 5×10^7 K.

(7) For the low-temperature component and SHTC in the decay phase super-hot event, the ratio of the two electron temperatures is about 1/5 to 1/2, and the ratio of the two emission measures is about 10^2 to 10^3.

5. Discussion

The decay phase SHTC has been identified by X-ray observations with spectrometers and hard X-ray imaging experiments. The general properties of the decay phase SHTC deduced from the ISEE-3 proportional counter measurements were summarized in the last section. Any mechanism which will be responsible for producing the decay phase SHTC should satisfy the following characteristics:

(1) Since the decay phase SHTC and low-temperature component have different histories (Figures 6d and 7c) and exist for a long time simultaneously without evidence for mixing, it seems that these two components exist in different coronal loops and are confined by magnetic field lines.

(2) For the SHTC, the important energy loss mechanism is heat conduction. Duijveman (1983) studied the heat balance for the SHTC of a solar flare and pointed out that the mean free path of an electron in the SHTC was comparable to the size of the super-hot source. The heat loss by conduction cannot be described by classical theory. For an SHTC, the characteristic cooling time caused by saturated heat conduction is much shorter than the duration (Duijveman, 1983). It is clear that the input of energy is required to maintain the decay phase SHTC. This is coincident with the pattern of energy content shown in Figure 6e.

(3) The fluctuations in the decay phase SHTC show that a periodic input of energy is more favored than continuous input, and the electron density or volume of the super-hot plasma source will increase with each input of additional energy.

Kopp and Pneuman (1976) proposed a reconnection mechanism to explain the formation of the post-flare loop prominence system. During the disruptive phase of the flare, the closed magnetic field lines open through the sudden release of mass and energy. Then an unbalanced Lorentz force drives field lines toward the neutral sheet and reconnection of magnetic field lines begins to take place, proceeding upward from the coronal base. During the reconnection process, the neutral point of field lines is rising vertically and a slow MHD shock wave is excited. Below the shocks there lies a hot, compressed loop which is composed of the most recently closed flux tubes. Below the hot loop, there is a loop of plasma that has cooled. Each appearance of new closed flux tubes is accompanied with the production of a new hot loop and a cooled loop. Cargill (1982) discussed the post-flare loops heated by the slow MHD shock wave and pointed out that if the velocity of shock propagation approaches the Alfvén speed, temperatures of 10^8 K can be produced.

The Kopp–Pneuman (K–P) model has been successfully applied to a large, long-lasting two-ribbon flare of July 29, 1973 to explain the continual formation of successively larger X-ray loops in the decay phase (Moore *et al.*, 1980) and to an impulsive, two-ribbon flare of May 21, 1980 to explain the location of the hot plasma region above a cool one just after the impulsive phase (Hoyng *et al.*, 1981).

Of the 35 events analyzed in this paper, 31 events have an associated Hα flare reported in *Solar Geophysical Data*. The absence of an associated Hα flare for four events is probably due to no flare patrol for those periods. Except for four events reported as 1B flares, all of the analyzed events are subflares. Of the four 1B flares three have an SHTC in the decay phase.

According to the qualitative understanding of the reconnection mechanism for post-flare loops as described above, and the properties of the SHTC in the decay phase obtained from the analyzed events, it appears that the K–P reconnection model may account for the formation of SHTC's in the decay phase. That is, a certain amount of magnetic energy is transformed into plasma heat energy to produce the SHTC by the shocks associated with the reconnection process, even if the overall scenario might be different from the large and long duration events usually described by this model. Thus the reconnection mechanism seems to be able to explain the continual formation of X-ray loops, the location of the two thermal components, and the production of SHTC's in the decay phase.

It seems that SHTC's may occur commonly in solar flares, especially in intense flares. It may be possible that an SHTC appears at the impulsive phase of a flare due to the process of chromospheric evaporation. Obviously, high energy and spatial resolution measurements are required for an unambiguous determination of the spectra of the non-thermal (power-law) component as well as the thermal component.

Acknowledgements

This work was done while H. Lin was at UC Berkeley as a visiting scholar from the People's Republic of China. The research at UC Berkeley was supported by the National Aeronautic and Space Administration under contract NAS 5–25980 and grant NAG 5–376.

References

Acton, L. W., Catura, R. C., and Roethig, D. T.: 1977, *Astrophys. J.* **218**, 881.
Anderson, K. A., Kane, S. R., Primbsch, J. H., Weitzmann, R. H., Evans, W. D., Klebesadel, R. W., and Aiello, W. P.: 1978, *IEEE Trans. Geosci. Electron.* **GE-16**, 157.
Arnoldy, R. L., Kane, S. R., and Winckler, J. R.: 1968, *Astrophys. J.* **151**, 711.
Bhalla, C. P., Gabriel, A. H., and Presnyakov, L. P.: 1975, *Monthly Notices Roy. Astron. Soc.* **172**, 359.
Brown, J. C.: 1972, *Solar Phys.* **25**, 158.
Brown, J. C.: 1975, in S. R. Kane (ed.), Solar Gamma, X-, and EUV Radiation', *IAU Symp.* **68**, 245.
Cargill, P. J. and Priest, E. R.: 1982, *Solar Phys.* **76**, 357.
Chubb, T. A., Kreplin, R. W., and Friedman, H. F.: 1966, *J. Geophys. Res.* **71**, 3611.
Culhane, J. L. and Acton, L. W.: 1970, *Monthly Notices Roy. Astron. Soc.* **151**, 141.
Duijveman, A.: 1983, *Solar Phys.* **84**, 189.
Hoyng, P., Duijveman, A., Machado, M. E., Rust, D. M., Švestka, Z., and 7 co-authors: 1981, *Astrophys. J. Letters* **246**, L155.
Jacobs, V. L., Davis, J., Kepple, P. C., and Blaha, M.: 1977, *Astrophys. J.* **211**, 605.
Kane, S. R., Fenimore, E. E., Klebesadel, R. W., and Laros, J. G.: 1982, *Astrophys. J. Letters* **254**, L57.
Kopp, R. A. and Pneuman, G. W.: 1976, *Solar Phys.* **50**, 85.
Lin, R. P. and Hudson, H. S.: 1971, *Solar Phys.* **17**, 412.
Lin, R. P. and Hudson, H. S.: 1976, *Solar Phys.* **50**, 153.
Lin, R. P., Schwartz, R. A., Pelling, R. M., and Hurley, K. C.: 1981, *Astrophys. J. Letters* **251**, L109.
Machado, M. E., Duijveman, A., and Dennis, B. R.: 1982, *Solar Phys.* **79**, 85.
Merts, A. L., Cowan, R. D., and Magee, N. H.: 1976, Los Alamos Scientific Laboratory Report No. LA-6220-MS.
Moore, R., McKenzie, D. L., Švestka, Z., Widing, K. G., and 12 co-authors: 1980, in P. A. Sturrock (ed.), *Solar Flares*, Colorado University Press, Boulder, p. 341.
Ohki, K., Takakura, T., Tsuneta, S., and Nitta, N.: 1983, *Solar Phys.* **86**, 301.
Parkinson, J. H., Veck, N. J., Ashfield, M. E. C., Culhane, J. L., Ku, W. H. M., Lemen, J. R., Noviek, R., Acton, L. W., and Wolfson, C. J.: 1979, *Astrophys. J.* **231**, 551.
Van Beek, H. F., Hoyng, P., Lafleur, H., and Simnett, G. M.: 1980, *Solar Phys.* **65**, 39.